Practical self-calibration of pan-tilt cameras

H.Kim and K.S.Hong

Abstract: The authors propose a practical self-calibration method of rotating and zooming cameras. The problem with previous methods occurs when the camera motion is almost fully zoomed with very little rotation, which is called the 'near-degenerate' configuration. In that case, the solutions become unstable and rotation angles cannot be calculated. When a pan-tilt camera (without z-axis rotation) is adopted and the intrinsic camera parameters are simplified, the near-degenerate configuration can be overcome and a closed-form solution obtained. Because pan-tilt cameras can be assumed for most stationary cameras (i.e. without translation) and the assumptions about the intrinsic camera parameters do not seem to effect the self-calibration, the method provides a simple, practical solution to the self-calibration problem. In addition, the authors introduce a nonlinear algorithm that adjusts not only the camera parameters but also the inter-image homography so that more accurate image registration is made possible. Simulations and experiments with real images are presented.

1 Introduction

In this paper, we deal with the self-calibration problem of rotating and zooming cameras. Hartley [1] has introduced a linear self-calibration method for rotating cameras with constant intrinsic parameters. Szeliski and Shum [2] have proposed a robust algorithm and applied it to solve the problem of image mosaicing. Some authors have extended Hartley's method to the self-calibration of rotating cameras with varying intrinsic parameters and proposed linear and nonlinear methods [3–6]. The problem for those methods occurs when the camera motion has almost completely zoomed with very little rotation, which we call the near-degenerate configuration. In that case, solutions become unstable and rotation angles cannot be calculated because the focal lengths are first estimated from inter-image homography, and then based on them, the rotation angles are calculated.

We found that when we adopt a pan-tilt camera (without z-axis rotation) and simplify the intrinsic camera parameters, we can overcome the near-degenerate configuration and can obtain a closed-form solution. In contrast to the previous approaches, rotation angles are calculated first and then the focal lengths are calculated, thereby overcoming the near-degenerate configuration. Because pan-tilt cameras can be assumed for most stationary cameras (i.e. without translation) and the assumptions about the intrinsic camera parameters do not seem to effect the self-calibration, our method provides a simple, practical solution to the self-calibration problem.

All previous algorithms use the following two steps for self-calibration. First, the inter-image homography is computed from matching points (or matching lines). Secondly the algorithm is performed using the estimated homography. Therefore, self-calibration methods depend on the inter-image homography estimation. That is, all previous algorithms are sensitive to the homography estimation. To improve the performance for real images, we merged the two steps into one using the Levenberg–Marquardt nonlinear optimisation in [7]. Our nonlinear algorithm adjusts not only camera parameters but also inter-image homography so that more accurate image registration can be achieved.

2 Self-calibration

2.1 Previous approaches

We consider rotating and zooming cameras with projection matrices $\boldsymbol{P}_k = \boldsymbol{K}_k[\boldsymbol{R}_k|\boldsymbol{0}]$, where $\boldsymbol{R}_k$ denotes the rotation of the kth camera with respect to the reference (0th) camera and $\boldsymbol{K}_k$ is the camera calibration matrix defined by

$$\boldsymbol{K}_k = \begin{bmatrix} \gamma_k f_k & s_k & x_0 \\ & f_k & y_0 \\ & & 1 \end{bmatrix} \tag{1}$$

where f_k represents the focal length, γ_k represents the aspect ratio, s_k represents the skew and (x_0, y_0) is called the principal point. When we only use two images, the camera parameters can be estimated using three assumptions: the zero-skew constraint ($s_k = 0$), or the square-pixel constraint ($\gamma_k = 1$) or the known principal point constraint [4, 6]. At least one of these constraints should be used to estimate camera parameters. In this paper, since the aspect ratio is usually known to be 1 or available from the spec-sheet of the camera, we assume the camera with the square-pixels.

For this camera model there exists a 2-D projective transformation $\boldsymbol{H}_k$, which transfers image points $\boldsymbol{u}_0$ on the reference frame to their matching points $\boldsymbol{u}_k$ on the kth frame, whose matrix is of the form

$$\boldsymbol{H}_k = \boldsymbol{K}_k \boldsymbol{R}_k \boldsymbol{K}_0^{-1} \tag{2}$$

IEE Proceedings online no. 20010574

DOI: 10.1049/ip-vis:20010574

Paper first received 26th October 1999 and in revised form 26th April 2000

The authors are with the Department of Electronics and Electrical Engineering, Pohang University of Science and Technology, Pohang, 790-784, Korea

The matrix is called an inter-image homography and it satisfies the relationship $\boldsymbol{u}_k = \boldsymbol{H}_k \boldsymbol{u}_0$, where $\boldsymbol{u}_k$ and $\boldsymbol{u}_0$ are matching points. For matching lines $\boldsymbol{l}_k$ and $\boldsymbol{l}_0$, the relationship $\boldsymbol{l}_k = \boldsymbol{H}_k^{-T} \boldsymbol{l}_0$ is satisfied.

From eqn. 2, some authors have proposed self-calibration methods that first estimate the focal lengths from inter-image homography and then calculate the rotation angles based on them [4, 6]. In [4] and [6], the authors propose two different linear calibration methods. Since the methods are similar, we only summarise the linear method of [6].

Since $\boldsymbol{R}_k \boldsymbol{R}_k^T = \boldsymbol{I}$, we can rewrite eqn. 2 as

$$\boldsymbol{H}_k \boldsymbol{K}_0 \boldsymbol{K}_0^T \boldsymbol{H}_k^T = \boldsymbol{K}_k \boldsymbol{K}_k^T \tag{3}$$

In addition to the square-pixel condition, the authors assumed that the principal points of the cameras are image centres ($(x_0, y_0) = (0, 0)$), the skews are zero ($s_k = 0$). These assumptions are reasonable because mislocating the principal points and zero-skew modelling does not seem to affect the self-calibration on the practical level. (The error due to our simplified camera modelling will be discussed in Section 2.4.) Eqn. 1 can be written as

$$\boldsymbol{K}_k = \mathrm{diag}(f_k, f_k, 1) \tag{4}$$

After some algebraic calculation, we have three equations to compute f_0

$$f_0^2(h_{11}h_{21} + h_{12}h_{22}) = -h_{13}h_{23} \tag{5}$$

$$f_0^2(h_{11}h_{31} + h_{12}h_{32}) = -h_{13}h_{33} \tag{6}$$

$$f_0^2(h_{21}h_{31} + h_{22}h_{32}) = -h_{23}h_{33} \tag{7}$$

and f_k can be computed using two equations

$$f_k^2 = \frac{f_0^2(h_{11}^2 + h_{12}^2) + h_{13}^2}{f_0^2(h_{31}^2 + h_{32}^2) + h_{33}^2} \tag{8}$$

$$f_k^2 = \frac{f_0^2(h_{21}^2 + h_{22}^2) + h_{23}^2}{f_0^2(h_{31}^2 + h_{32}^2) + h_{33}^2} \tag{9}$$

where $\boldsymbol{H}_k = [h_{ij}]$. Note, however, that when the x-axis is the rotation axis, only eqn. 7 of eqns. 5–7 is valid, and when the y-axis is the rotation axis, only eqn. 6 is valid. To handle these special cases the authors checked the image motion direction using matching points and chose which equation is valid according to the average of the image motion directions. The rotation matrix $\boldsymbol{R}_k$ can be written as

$$\boldsymbol{R}_k = \frac{\boldsymbol{K}_k^{-1} \boldsymbol{H}_k \boldsymbol{K}_0}{\det(\boldsymbol{K}_k^{-1} \boldsymbol{H}_k \boldsymbol{K}_0)^{1/3}} \tag{10}$$

and the rotation angles can be decomposed from it using the singular value decomposition. Theoretically, the calibration of the focal lengths and the rotation is unique up to an orthogonal transformation, assuming that the skew of the camera is zero [5]. That is, the calibration is unique if the reference frame is fixed in the above camera model.

The problem with the above methods occurs when the camera motion is in the near-degenerate configuration. In that case, the solutions become unstable and the rotation angles cannot be calculated.

2.2 Near-degenerate configuration

If $\boldsymbol{R}_k = \boldsymbol{I}$ (zero rotation case, i.e. the degenerate configuration), eqns. 5–7 become $f_0^2(0 + 0) = 0$, and f_0 and f_k cannot be estimated. Therefore, when a camera purely zooms without rotation, only the ratio of f_0 and f_k can be estimated. In addition, the same problem occurs when camera motion is in the near-degenerate configuration. In that case, the previous approaches provide unstable solutions and the rotation angles cannot be calculated. However, for a pan-tilt camera the rotation angles can be estimated even in the near-degenerate configuration.

2.3 Self-calibration of a pan-tilt camera with varying focal lengths

We now propose a new method for a special camera configuration, that is, a pan-tilt camera (without z-axis rotation), which we can assume for most stationary cameras (i.e. without translation). Our camera matrix is represented by eqn. 4, which is used in Seo and Hong's linear algorithm [5]. In contrast to the previous approaches, the rotation angles are calculated first, and then the focal lengths are calculated, thereby overcoming the near-degenerate configuration.

Because we focus on the self-calibration of pan-tilt cameras, eqn. 2 can be written as

$$\boldsymbol{H}_k(f_0, f_k, \alpha_k, \beta_k) = \begin{bmatrix} \cos\beta_k & \sin\alpha_k \sin\beta_k & -\cos\alpha_k \sin\beta_k f_0 \\ 0 & \cos\alpha_k & \sin\alpha_k f_0 \\ \sin\beta_k / f_k & -\dfrac{\sin\alpha_k \cos\beta_k}{f_k} & \cos\alpha_k \cos\beta_k f_0 / f_k \end{bmatrix} \tag{11}$$

where α_k and β_k are the rotation angles around the x-axis and the y-axis of the reference camera coordinate, respectively. We assume that the rotation angle around the z-axis is negligibly small. Note that, as in the previous approaches, we set the reference frame at the camera coordinate of the 0th camera so that the pan-tilt angles, i.e. α_0 and β_0, are zero. In this case, the number of unknowns is four: two for rotation and two for focal length. One inter-image homography $\boldsymbol{H}_k$ from which we have eight equations is sufficient to compute the unknown parameters.

From eqn. 11 we obtain equations to compute α_k and β_k by eliminating f_0 and f_k

$$\alpha_k = \frac{h_{23}h_{33}}{|h_{23}h_{33}|} \tan^{-1} \sqrt{\left| \frac{h_{23}h_{32}}{h_{22}h_{33}} \right|} \tag{12}$$

$$\beta_k = -\frac{h_{13}h_{33}}{|h_{13}h_{33}|} \tan^{-1} \sqrt{\left| \frac{h_{13}h_{31}}{h_{11}h_{33}} \right|} \tag{13}$$

f_0 and f_k can also be directly computed from inter-image homography:

$$\begin{cases} f_0 = \sqrt{|h_{13}h_{33}/(h_{11}h_{31} + h_{12}h_{32})|}, & \text{if } |\alpha_k| \le |\beta_k| \\ f_0 = \sqrt{|h_{23}h_{33}/(h_{21}h_{31} + h_{22}h_{32})|}, & \text{elsewhere} \end{cases} \tag{14}$$

$$f_k = \frac{1}{2}\left(\sqrt{\frac{f_0^2(h_{11}^2 + h_{12}^2) + h_{13}^2}{f_0^2(h_{31}^2 + h_{32}^2) + h_{33}^2}} + \sqrt{\frac{f_0^2(h_{21}^2 + h_{22}^2) + h_{23}^2}{f_0^2(h_{31}^2 + h_{32}^2) + h_{33}^2}} \right) \tag{15}$$

When $h_{11}h_{31} + h_{12}h_{32} = 0$ (ideal pure zooming case), the focal lengths have no solution. In this case we let f_0 be an arbitrary nonzero constant and f_k is determined from eqn. 15. We can see that eqns. 12–15 give a simple, closed form solution.

We conclude that all the camera parameters are estimated directly from the inter-image homography for a pan-tilt camera with varying focal lengths. Note that the focal lengths themselves are not stable but the ratio of the focal

lengths is stable in the neighbourhood of the degenerate configuration. Simulation results will support this point in Section 4.1.

2.4 Error analysis due to the simplification of camera modelling

We simplify intrinsic camera parameters to overcome the near-degenerate configuration and obtain a closed form solution. However, real cameras with zoom lenses need more complex modelling such as assuming a nonzero principal point and lens distortion modelling.

Willson [8] stated that while there is no problem in fixing the aspect ratio and the skew of the pixel coordinate axes, which are very stable over long time periods, the position of the principal point depends on the zooming position and lens focus of the camera. Therefore, the error analysis of the zero assumption of principal points is needed. We give a brief summary here, see [6] for more details.

Since we do not know the exact principal point, the intrinsic camera matrices $\boldsymbol{K}_i$, $i=0, k$, will have some deviation from the truth

$$\tilde{\boldsymbol{K}}_i = \boldsymbol{K} + \boldsymbol{K}_\Delta = \begin{bmatrix} f_i & & \\ & f_i & \\ & & 1 \end{bmatrix} + \begin{bmatrix} 0 & 0 & \Delta_x \\ 0 & 0 & \Delta_y \\ 0 & 0 & 0 \end{bmatrix} \quad (16)$$

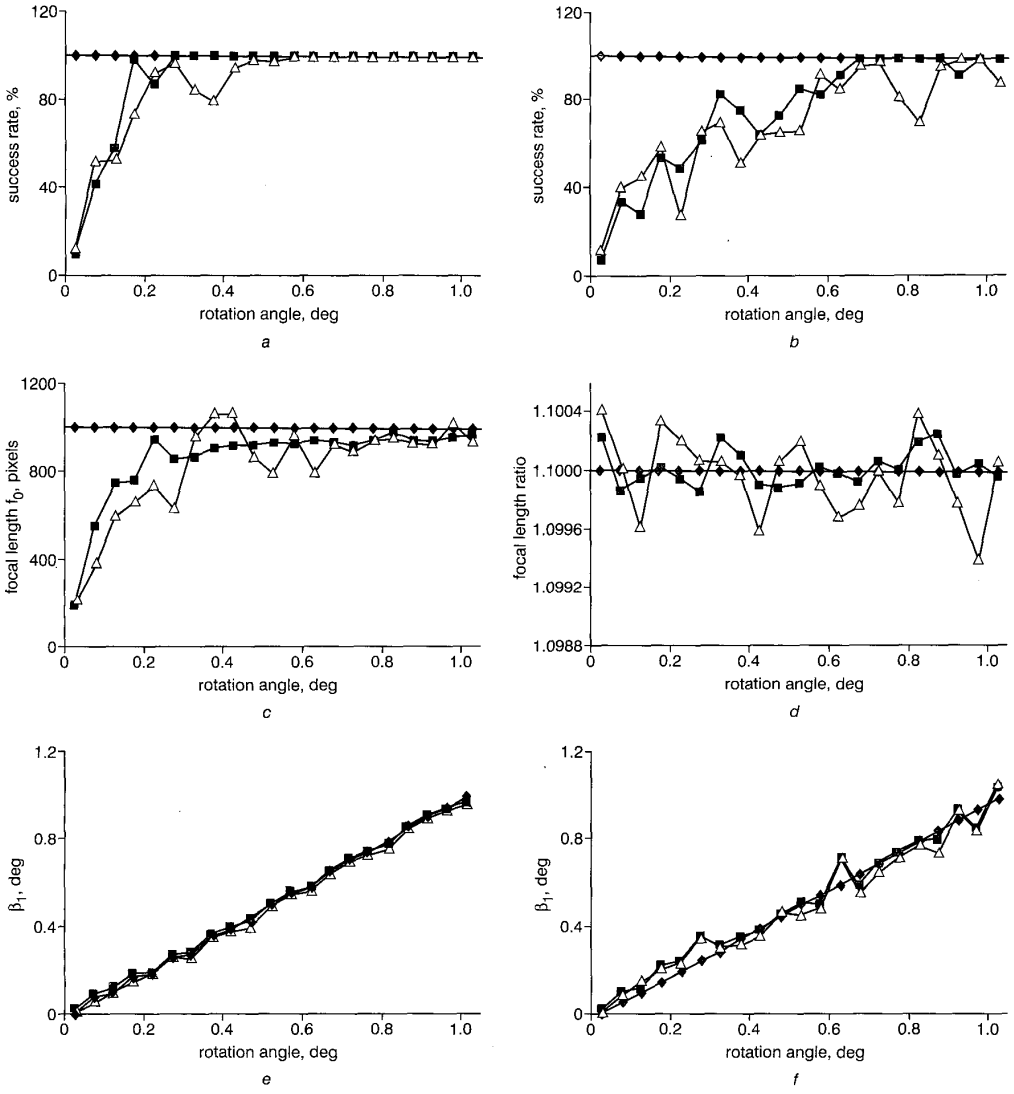

Fig. 1 *Simulation results*

a Success rates of two self-calibration methods at noise levels of 0.5 and 1.0 pixels
—◆— proposed; —■— previous (0.5); —△— previous (1.0)
b Success rates at noise levels of 1.5 and 2.0 pixels
—◆— proposed; —■— previous (1.5); —△— previous (2.0)
c Mean of focal length f_0
—◆— ground truth; —■— previous (0.5); —△— previous (1.0)
d Mean of focal length ratio f_1/f_0
—◆— ground truth; —■— previous (0.5); —△— previous (1.0)
e Mean of rotation angle β_1 at noise level of 0.5 pixel
—◆— ground truth; —■— previous (0.5); —△— proposed (0.5)
f Mean of rotation angle β_1 at noise level of 1.0 pixels
—◆— ground truth; —■— previous (0.5); —△— proposed (0.5)

When we assume that the rotation angle α_k is larger than β_k, we have an estimation of $\hat{f}_0$ through the Taylor series expansion

$$\frac{\hat{f}_0^2}{f_0^2} \approx 1 + \frac{\Delta_y}{\tan \alpha_k}\left(\frac{1}{f_0} - \frac{\cos \beta_k}{f_k}\right) \tag{17}$$

It says that the more the focal length changes due to the zoom operation of the camera, the larger is the effect of the principal point error. Conversely, if the focal length change is small, the error may be negligible. From the same reasoning, the larger the rotation angle is, the smaller the effect of the principal point error is. For example, when $f_0 = 1000$, $f_k = 900$, $\Delta_y = 20$ pixel and $\alpha_k = 3°$, we have about 2.1% deviation in the estimations $\hat{f}_0$ and $\hat{f}_k$ from the truth value.

The other significant error source is nonlinear lens distortion which can be removed before calibration by using some algorithms like those given in [9, 10].

3 Improvement of inter-image homography

All previous algorithms use the following two steps for self-calibration. First, inter-image homography is computed from matching points (or matching lines), and secondly, the algorithm is performed using the estimated homography. Therefore, self-calibration methods depend on the inter-image homography estimation. That is, previous algorithms, including our proposed linear self-calibration algorithm, are sensitive to the homography estimation. To improve the performance for real images, we merge the two steps into one using a nonlinear optimisation. The nonlinear algorithm can improve inter-image homography due to the parameterisation of the camera parameters.

Our approach is to estimate the camera parameters directly from matching points, not from the result of inter-image homography estimation. The relationship between M matching points, $\boldsymbol{u}_k = \{\boldsymbol{u}_k^1, \ldots, \boldsymbol{u}_k^M\}$ and $\boldsymbol{u}_0 = \{\boldsymbol{u}_0^1, \ldots, \boldsymbol{u}_0^M\}$, is $\boldsymbol{u}_k = \boldsymbol{H}_k \boldsymbol{u}_0$. Remember that the inter-image homography is parameterised by the camera parameters f_0, f_k, α_k and β_k (eqn. 11). To solve the camera

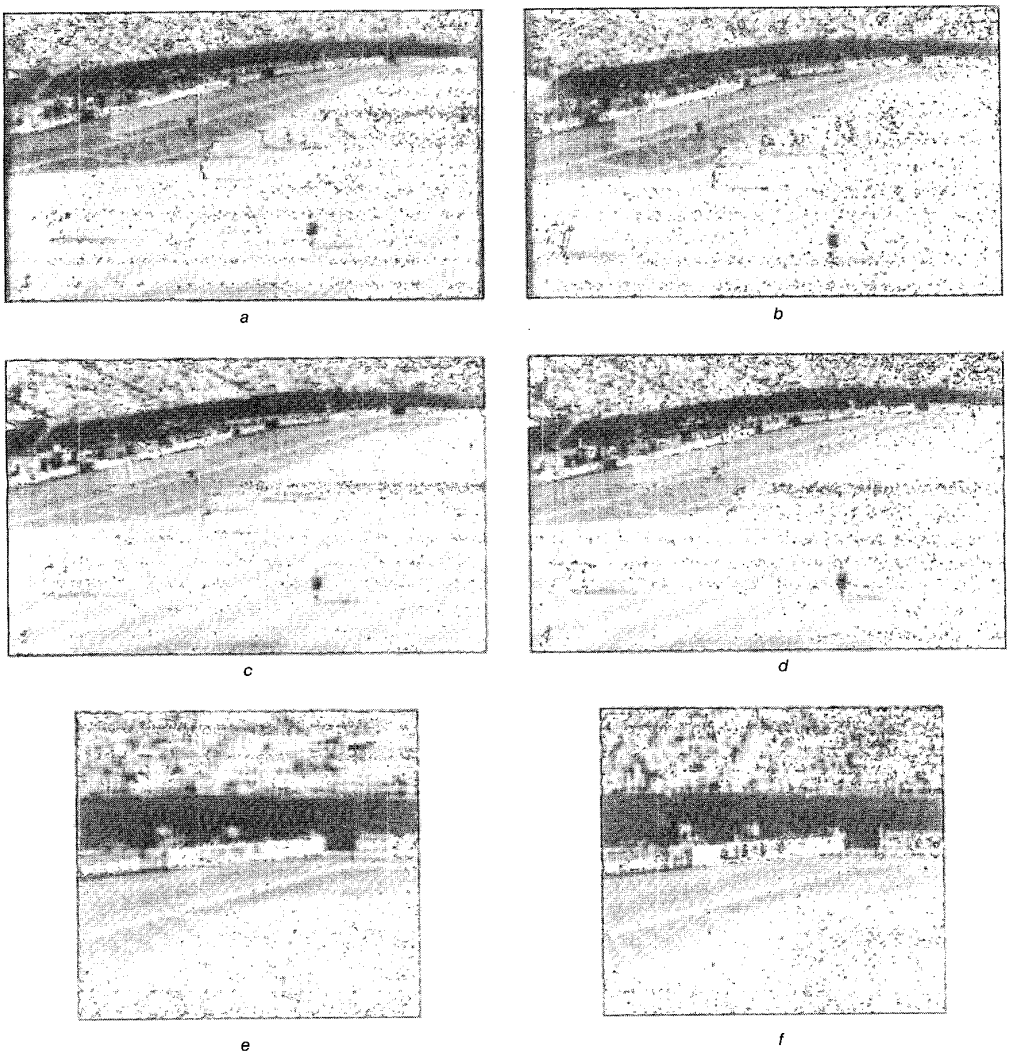

Fig. 2 *Self-calibration performance comparison*

a, b Original image pair
c, d Merged images by homography and the refined homography
e, f Magnified parts of *c* and *d*

parameters and the inter-image homography simultaneously, we minimise the following error function with respect to the camera parameters:

$$\boldsymbol{E}(f_0, f_k, \alpha_k, \beta_k) = \frac{1}{M}\sum_{i=1}^{M} \| \boldsymbol{u}_k^i - \boldsymbol{H}_k(f_0, f_k, \alpha_k, \beta_k)\boldsymbol{u}_0^i \|^2 \tag{18}$$

That is, we minimise the Euclidean distance between corresponding points.

For matching lines $\boldsymbol{l}_0 = \{\boldsymbol{l}_0^1, \ldots, \boldsymbol{l}_0^M\}$ and $\boldsymbol{l}_k = \{\boldsymbol{l}_k^1, \ldots, \boldsymbol{l}_k^M\}$, the equation has the form

$$\boldsymbol{E} = \frac{1}{M}\sum_{i=1}^{M}\left[\frac{\mathrm{d}(\boldsymbol{l}_k^i, \boldsymbol{H}_k^{-T}\boldsymbol{l}_0^i) + \mathrm{d}(\boldsymbol{l}_0^i, \boldsymbol{H}_k^T\boldsymbol{l}_k^i)}{2}\right]^2 \tag{19}$$

where $\mathrm{d}(\boldsymbol{l}_a, \boldsymbol{l}_b)$ denotes the distance between two lines, $\boldsymbol{l}_a$ and $\boldsymbol{l}_b$. We call it the matching error. When the two endpoints of $\boldsymbol{l}_a$ are $\boldsymbol{e}_a^1$ and $\boldsymbol{e}_a^2$, and $\boldsymbol{l}_b$ has the form $(\boldsymbol{l}_{b,1}, \boldsymbol{l}_{b,2}, \boldsymbol{l}_{b,3})^T$ in the homogeneous coordinate, the distance is defined by

$$\mathrm{d}(\boldsymbol{l}_a, \boldsymbol{l}_b) = \frac{\sqrt{|\boldsymbol{l}_b^T\boldsymbol{e}_a^1|^2 + |\boldsymbol{l}_b^T\boldsymbol{e}_a^2|^2}}{(\boldsymbol{l}_{b,1}^2 + \boldsymbol{l}_{b,2}^2)} \tag{20}$$

The distance measure between matching lines is only an example and other distance measures can be used. The linear solution (Section 2.3) is used for initial values and then eqn. 18 or eqn. 19 is optimised by the Levenberg–Marquardt method [11]. This nonlinear method improves inter-image homography and refines the linear solution simultaneously.

4 Experimental results

We now compare the performance of the linear self-calibration method to earlier methods. Seo and Hong's linear method [6] is selected as a representative of the

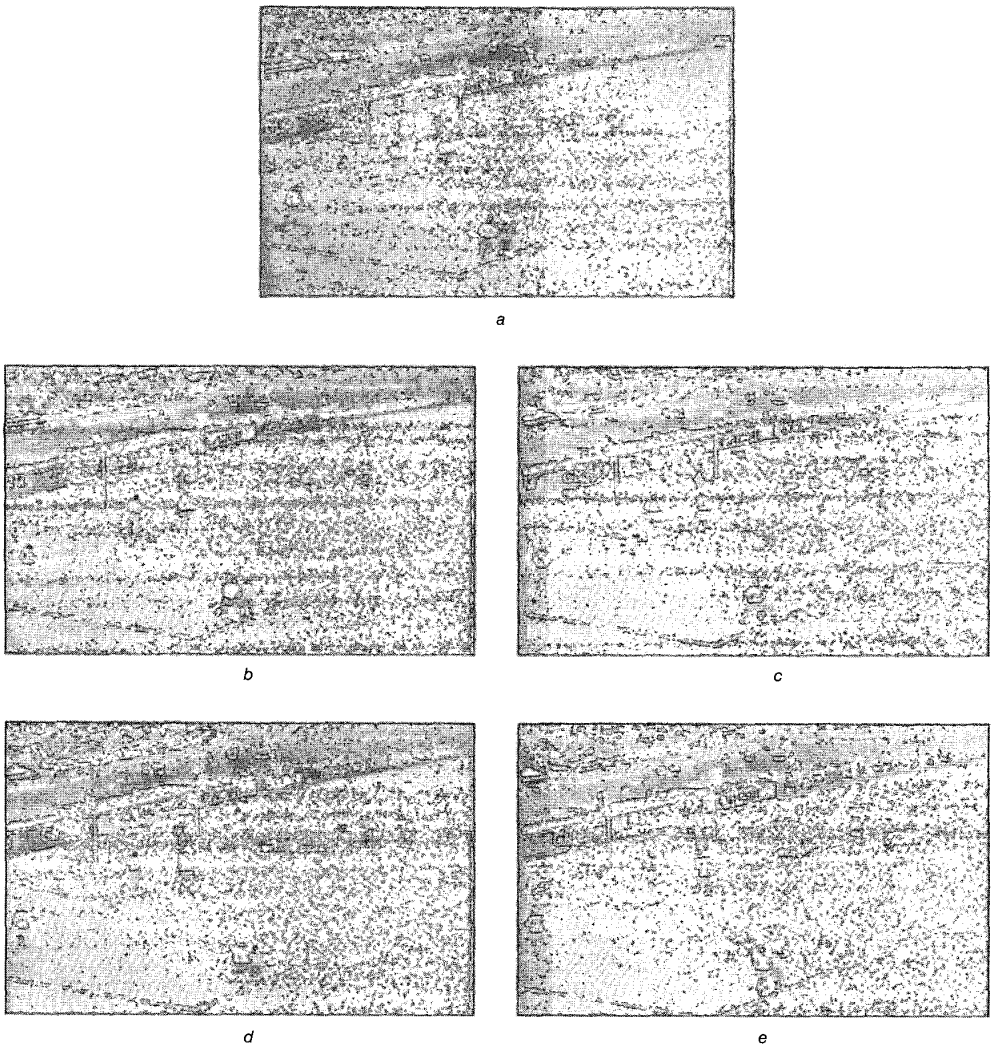

Fig. 3 *Original soccer video*
a Reference image
b First frame
c Second frame
d Third frame
e Last frame

earlier methods. We will show the results of the linear method in this simulation and the performance of the nonlinear method will be shown in Section 4.2 by applying it to real images.

4.1 Simulation

An image S_0 with size 500×500 pixels is chosen as a reference image and points $\{u_0^i,\ i=1,\ldots,M\}$ on the sampled grid in the image are selected as feature points. Then the feature points are transferred into image S_1 using inter-image homography synthesised from our given camera parameters. The transferred points $\{u_1^i,\ i=1,\ldots,M\}$ in image S_1 and their corresponding points in image S_0 are used as matching pairs. Among them, 100 pairs are randomly selected and they are represented by $u_1=\{u_1^i,\ i=1,\ldots,100\}$ and $u_0=\{u_0^i,\ i=1,\ldots,100\}$. Gaussian noise of standard deviation σ (pixels) is added to the matching points between the two images to both sides.

We repeated 100 computations using randomly generated Gaussian noise. The focal lengths are $f_0=1000$ pixels and $f_1=1100$ pixels. The two rotation angles α_1 and β_1 simultaneously vary from 0° to 1° with a step size of 0.05°. Experiments are done for four noise levels: $\sigma=0.5$, 1.0, 1.5 and 2.0.

For cameras with very small rotation, the calculated values become very unstable and we cannot obtain results in the following two cases. One is when the focal length f_0 cannot be calculated from eqns. 5–7 because $f_0^2<0$. The other is when the rotation angles cannot be recovered because the trigonometric functions contained in the equations are beyond their range, say, greater than 1 or less than −1. We call the two cases failures. Using 100 attempts we counted the success rate of self-calibration methods and used it as a measure of stability. Figs. 1*a* and *b* show the success rates. We can see that our proposed linear method shows 100% success even for small rotation angles, while the earlier method does not. The plot shows that when the noise level increases, the range where failures occur increases. At noise levels of 0.5 and 1.0 pixels, the failures occur until 0.25° and 0.55°, respectively. At noise levels of 1.5 and 2.0 pixels, the self-calibration results are unstable even at a rotation angle of 1.0°.

Figs. 1*c–f* present estimated camera parameters. The estimations of both the focal lengths and their ratio by the two methods are the same for the successful case; hence, we show only the result of the proposed method in Figs. 1*c* and *d*. For small angles our method did not correctly estimate the exact values of the focal length f_0, but the ratio of the focal lengths is stably estimated. Figs. 1*e* and *f* show the result of the rotation angle estimation at the two noise levels and they tell us that our method is comparable with earlier methods.

4.2 Experiments with real images

We now show the performance of our nonlinear self-calibration method using two experiments. In the first experiment, we show that our method can refine the estimation of inter-image homography. The second experiment shows the performance for a video segment.

First, let us show that our method can refine the estimation of inter-image homography and give a reasonable

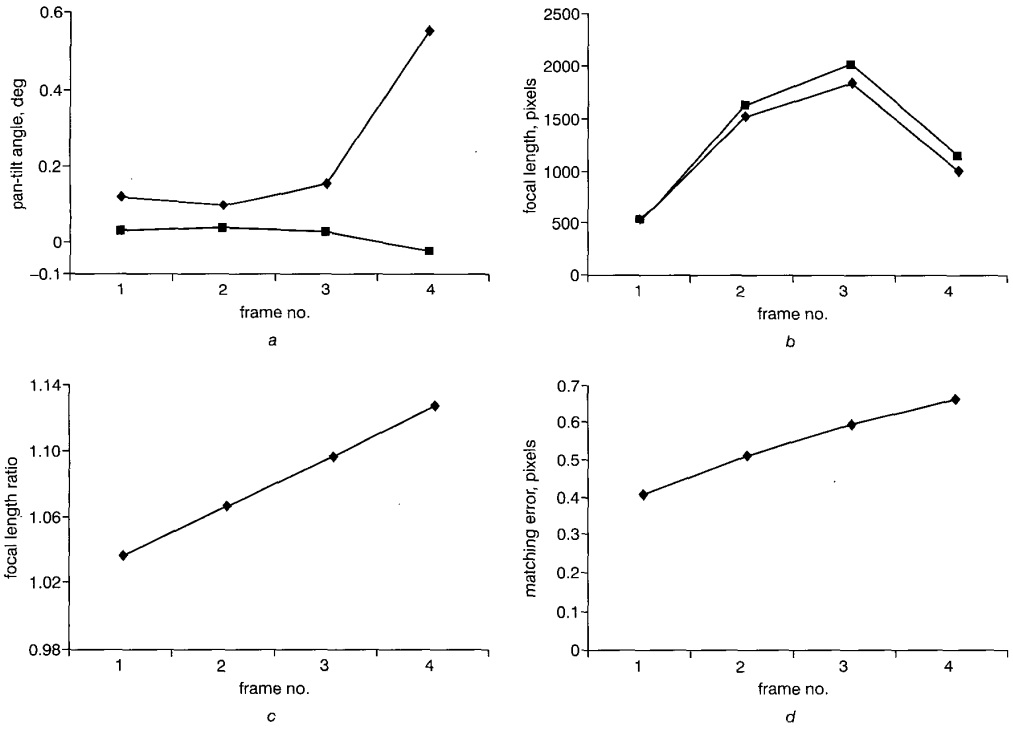

Fig. 4 *Estimated camera parameters with respect to the reference frame*

a Rotation angles
—◆— tilt angle; —■— pan angle
b Focal lengths
—◆— f_0; —■— f_1
c Focal length ratio
d Matching error

solution even for a camera with little rotation. Figs. 2*a* and *b* are the original image pair. Line features are extracted from the images and they are matched using a proximity rule. The matching lines are refined by the least median squares (LMedS) method [12] and an inter-image homography is estimated from the refined matching lines. The number of matching lines by the proximity rule was 72 and the number of refined matching lines was 65. The merged image using this homography is shown in Fig. 2*c*. The pixels in the overlapped region are merged by averaging their intensity values. The image is somewhat blurred, and misregistration on the advertising board and the auditorium is noticeable.

Then, from the refined matching lines we estimate a refined inter-image homography using our nonlinear self-calibration method. The merged image is presented in Fig. 2*d*. Figs. 2*e* and *f* show the magnified parts of Figs. 2*c* and 2*d*, respectively. You can see that the advertising board and auditorium are sharply registered, as well as the lines on the playing field. Therefore, the experiment shows that our nonlinear method has the ability to reline inter-image homography and works well with noisy, real images. The estimated parameters are $f_0 = 1119.84$, $f_1 = 1202.13$, $\alpha_1 = 0.84°$ and $\beta_1 = 0.57°$. Since the images seem to be zoomed in and rotated with positive angles, the estimated parameters seem to be reasonable.

In the second experiment, we apply our algorithm to a video segment and analyse the self-calibration result. In Fig. 3, the video sources are shown and the camera motion is almost fully zoomed with very little rotation for all the frames. The experimental procedure is the same as the first one. Fig. 3*a* is the reference image and other images are registered to it. Fig. 4 shows the self-calibration results. Fig. 4*a* shows the rotation angles calculated. Although their values are very small, i.e. less than 1°, the estimation seems to be reasonable. The focal lengths shown in Fig. 4*b* are incorrect, where f_0 should be constant for all frames, because the rotation angles are small. However, the ratio of the focal lengths seems to be correctly estimated (see Fig. 4*c*). Fig. 4*d* shows the quantitative analysis on the matching performance using the matching error (eqn. 19). We can see that our algorithm works well, even though the rotation angles are small.

5 Conclusions

We have proposed a simple, practical self-calibration method for a pan-tilt camera configuration, which we can assume for most stationary cameras. When we simplified the intrinsic camera parameters, we could overcome the near-degenerate configuration, where the solutions become unstable and rotation angles cannot be calculated using earlier methods. In addition, we have introduced a nonlinear algorithm which adjusts not only camera parameters but also inter-image homography so that more accurate image registration is made possible.

6 References

1 HARTLEY, R.I.: 'Self-calibration of stationary cameras', *Int. J. Comput. Vis.*, 1997, **22**, (1), pp. 5–23
2 SZELISK, R., and SHUM, H.Y.: 'Creating full view panoramic image mosaics and environment maps'. Proceedings of SIGGRAPH, 1997, pp. 251–258
3 DE AGAPITO, L., HAYMAN, E., and REID, I.: 'Self-calibration of a rotating camera with varying intrinsic parameters'. Proceedings of the British machine vision conference, 1998
4 DE AGAPITO, L., HARTLEY, R.I., and HAYMAN, E.: 'Linear calibration of a rotating and zooming camera'. Proceedings of the international conference on *Computer vision and pattern/recognition*, 1999, pp. I:15–21
5 SEO, Y., and HONG, K.S.: 'Auto-calibration of a rotating and zooming camera'. Proceedings of the IAPR workshop on *Machine vision applications*, 1998, pp. 274–277
6 SEO, Y., and HONG, K.S.: 'About the self-calibration of a rotating and zooming camera: theory and practice'. Proceedings of the international conference on *Computer vision*, 1999, pp. 183–188
7 HARTLEY, R.I.: 'Euclidean reconstruction from uncalibrated views'. Proceedings of the Second Europe–US Workshop on *Invariance*, 1993
8 WILLSON, R.G.: 'Modeling and calibration of automated zoom lenses'. CMU Robotics Institute Technical Report, 1994
9 SAWHNEY, H.S., and KUMAR, R.: 'True multi-image alignment and its application to mosaicing and lens distortion correction', *IEEE Trans., Pattern Anal. Mach. Intell.*, 1999, **21**, (3), pp. 235–243
10 DEVERNAY, F., and FAUGERAS, O.: 'Automatic calibration and removal of distortion from scenes of structured environments', *Proc. SPIE-Int. Soc. Opt. Eng.*, 1995, **2567**, pp. 62–72
11 PRESS, W.H., TEUKOLSKY, S.A., VETTERLING, W.T., and FLANNERY, B.P.: 'Numerical recipes in C: the art of scientific computing' (Cambridge University Press, 1993, 2nd edn.)
12 ZHANG, Z.: 'Parameter estimation techniques: a tutorial with application to conic fitting'. INRIA Technical Report RR-2676, 1995